JAMES | Journal of Advances in Modeling Earth Systems

RESEARCH ARTICLE
10.1029/2026MS005804

Exploring Air–Sea Interactions in a Regional Weakly Coupled Data Assimilation System: An Observing System Experiment for the 2023 Indian Ocean Monsoon and Cyclone Biparjoy

Rui Sun[1], Aneesh C. Subramanian[2], Matthew R. Mazloff[1], Sivareddy Sanikommu[3,4], Ganesh Gopalakrishnan[1], Bruce D. Cornuelle[1], Tien-Yiao Hsu[1], Arthur J. Miller[1], Prajeesh Ag[3,4], and Ibrahim Hoteit[3]

[1]Scripps Institution of Oceanography, La Jolla, CA, USA, [2]Department of Atmospheric and Oceanic Sciences, University of Colorado Boulder, Boulder, CO, USA, [3]Physical Sciences and Engineering Division, King Abdullah University of Science and Technology (KAUST), Thuwal, Saudi Arabia, [4]Climate Change Center, National Center for Meteorology, Jeddah, Saudi Arabia

Key Points:

- We implement a weakly coupled DA system for the Arabian Sea region to study the monsoon onset and cyclone Biparjoy in 2023
- Observing system experiments show the coupled DA system produces better forecasts when both oceanic and atmospheric data are assimilated
- Assimilating only oceanic data leads to warmer SST below the misplaced cyclone, increasing error in atmospheric state forecasts

Correspondence to:
R. Sun,
rus043@ucsd.edu

Citation:
Sun, R., Subramanian, A. C., Mazloff, M. R., Sanikommu, S., Gopalakrishnan, G., Cornuelle, B. D., et al. (2026). Exploring air–sea interactions in a regional weakly coupled data assimilation system: An observing system experiment for the 2023 Indian Ocean monsoon and cyclone Biparjoy. *Journal of Advances in Modeling Earth Systems*, *18*, e2026MS005804. https://doi.org/10.1029/2026MS005804

Received 3 FEB 2026
Accepted 19 OCT 2026

Author Contributions:
Conceptualization: Rui Sun, Aneesh C. Subramanian, Matthew R. Mazloff, Bruce D. Cornuelle, Ibrahim Hoteit
Data curation: Rui Sun, Sivareddy Sanikommu, Ganesh Gopalakrishnan, Prajeesh Ag
Formal analysis: Rui Sun, Aneesh C. Subramanian, Matthew R. Mazloff, Sivareddy Sanikommu, Ganesh Gopalakrishnan, Bruce D. Cornuelle, Tien-Yiao Hsu, Arthur J. Miller, Ibrahim Hoteit
Funding acquisition: Rui Sun, Aneesh C. Subramanian, Matthew R. Mazloff, Bruce D. Cornuelle, Ibrahim Hoteit

© 2026 The Author(s). Journal of Advances in Modeling Earth Systems published by Wiley Periodicals LLC on behalf of American Geophysical Union. This is an open access article under the terms of the Creative Commons Attribution-NonCommercial License, which permits use, distribution and reproduction in any medium, provided the original work is properly cited and is not used for commercial purposes.

Abstract We examined air–sea interactions in a weakly coupled ocean–atmosphere data assimilation (DA) system by performing an observing system experiment (OSE). The OSE is performed for the Arabian Sea monsoon onset event in 2023, which also coincides with the passage of the tropical cyclone Biparjoy. Results show that assimilating both oceanic and atmospheric data produces a better forecast of the ocean–atmosphere state (fit to the assimilated data) than either experiment assimilating only oceanic or atmospheric data. This indicates that the coupled system provides more consistent initial conditions, yielding more balanced oceanic and atmospheric states when assimilating all the data. However, we found that assimilating only atmospheric data improves both the ocean and atmosphere state forecasts, whereas assimilating only oceanic data improves the ocean state forecasts but degrades the atmospheric state forecasts, when compared with the free run (coupled model simulation without assimilating any data). We found that this counterintuitive model performance is due to the systematic misrepresentation of air–sea exchanges. First, errors in the cyclone path increase when atmospheric data are not assimilated. Then, assimilation of sea surface temperature (SST) leads to a warmer SST below the misplaced cyclone (with cyclone path offset of about 200 km relative to IBTrACS data), resulting in increased cyclone intensity. This misrepresentation of air–sea exchanges not only occurs during the cyclone passage but also persists throughout the early monsoon season. Since errors in one component can affect the other and result in positive feedback, leading to error growth, this study highlights an interesting effect on weakly coupled ocean–atmosphere DA systems when atmospheric data are unavailable or limited in space and time, particularly during high-impact atmospheric events such as tropical cyclones.

Plain Language Summary We examined air–sea interactions in a weakly coupled ocean–atmosphere data assimilation system. Experiments are performed to evaluate this system for the Arabian Sea monsoon onset in 2023, when tropical cyclone Biparjoy also occurred. Results show that assimilating both oceanic and atmospheric data produces better forecasts. However, using only oceanic data improves the ocean state forecasts but degrades the atmospheric state forecasts. We found that this counterintuitive behavior arises from the systematic misrepresentation of air–sea exchanges. First, the errors in the cyclone path increase in the model; then, assimilation of ocean temperature leads to a warmer ocean below the misplaced cyclone, resulting in an increased cyclone intensity. This shows that in the coupled system, errors in one component can amplify errors in the other. This study highlights an interesting effect on weakly coupled ocean–atmosphere data assimilation systems when atmospheric data are unavailable or limited, particularly during high-impact atmospheric events such as tropical cyclones.

1. Introduction

Ocean–atmosphere coupled models have been used extensively to simulate, understand, and predict the behavior of the Earth's system (Flato, 2011; Giorgi & Gao, 2018). Because these models can be different compared to observations at specific times and locations, data assimilation (DA) is used to constrain the model solutions using

Investigation: Rui Sun, Aneesh C. Subramanian, Matthew R. Mazloff, Sivareddy Sanikommu, Ganesh Gopalakrishnan, Bruce D. Cornuelle, Tien-Yiao Hsu, Arthur J. Miller, Ibrahim Hoteit
Methodology: Rui Sun, Aneesh C. Subramanian, Matthew R. Mazloff, Sivareddy Sanikommu, Ganesh Gopalakrishnan, Bruce D. Cornuelle, Tien-Yiao Hsu, Arthur J. Miller, Prajeesh Ag, Ibrahim Hoteit
Project administration: Aneesh C. Subramanian, Matthew R. Mazloff, Ganesh Gopalakrishnan, Bruce D. Cornuelle, Arthur J. Miller, Ibrahim Hoteit
Resources: Rui Sun, Aneesh C. Subramanian, Ganesh Gopalakrishnan, Bruce D. Cornuelle, Ibrahim Hoteit
Software: Rui Sun, Sivareddy Sanikommu, Ganesh Gopalakrishnan, Prajeesh Ag
Supervision: Aneesh C. Subramanian, Matthew R. Mazloff, Ganesh Gopalakrishnan, Bruce D. Cornuelle, Arthur J. Miller, Ibrahim Hoteit
Validation: Rui Sun
Visualization: Rui Sun, Sivareddy Sanikommu
Writing – original draft: Rui Sun, Aneesh C. Subramanian, Ganesh Gopalakrishnan
Writing – review & editing: Rui Sun, Aneesh C. Subramanian, Matthew R. Mazloff, Sivareddy Sanikommu, Ganesh Gopalakrishnan, Bruce D. Cornuelle, Tien-Yiao Hsu, Arthur J. Miller, Prajeesh Ag, Ibrahim Hoteit

observations by accounting for observation uncertainty and model representational error (Edwards et al., 2015; Laloyaux et al., 2016).

Recently, de Rosnay et al. (2022) summarized the large diversity of coupled model DA methodologies developed in various communities involved in numerical weather prediction (NWP), seasonal forecasts, and ocean DA (e.g., Browne et al., 2019; Fowler & Lawless, 2016; Frolov et al., 2016; Hoteit et al., 2018; Karspeck et al., 2018; Moore et al., 2019). Several NWP centers also use coupled DA systems for operational NWP and reanalysis applications, including the UK Met Office (Lea et al., 2015), the Japan Meteorological Agency (JMA, Fujii et al., 2021), and the European Centre for Medium-Range Weather Forecasts (ECMWF, Browne et al., 2019; de Rosnay et al., 2022; Schepers et al., 2018). Coupled DA aims at providing improved initial conditions across the coupled forecast model components (Laloyaux et al., 2016; Penny et al., 2017). It consists of exchanging information between DA systems so that observations from one component can influence the analysis of other component. Zhang et al. (2020) provided a comprehensive review of different coupling approaches, broadly categorized into two types: weakly coupled DA (WCDA) and strongly coupled DA (SCDA). This work also reviewed the studies that explored coupled DA in coupled ocean–atmosphere models for seamless weather–climate prediction on weekly-to-decadal time scales. For example, using a global coupled model, Browne et al. (2019) showed that the coupled DA system improved the prediction skill for the position of the summer monsoon, which is difficult to forecast. Recently, a clear improvement in surface stress during the Indian monsoon was also identified using a coupled DA system (de Rosnay et al., 2022).

To assess the potential advantages of the coupled DA system over uncoupled DA, we implement a coupled ensemble DA system for the Red Sea, the Arabian Gulf, and the Arabian Sea, and part of the Bay of Bengal using the Scripps–KAUST Regional Integrated Prediction System (SKRIPS, Sun et al., 2019, 2023) and the Data Assimilation Research Testbed (DART, J. Anderson et al., 2009; El Gharamti et al., 2025). Compared to our previous DA efforts (Sanikommu et al., 2020; Sun et al., 2024), in this study we extended the capability of the coupled system by (a) implementing the DART–WRF interface to assimilate atmospheric observations and (b) expanding the domain of the regional coupled model to include the Arabian Sea region. Assimilating the atmospheric observations allows us to assess their impact on air–sea interactions in the coupled DA experiment for this region. Using an atmospheric model with a higher resolution than the global model could also enhance the oceanic and atmospheric forecast performance. Moreover, compared to our previous assimilation experiments using ocean-only models with an ensemble of prescribed atmospheric states (Sanikommu et al., 2023, 2025), the present experiments using the coupled ocean–atmosphere model naturally provide an ensemble of atmospheric states.

To evaluate the impact of assimilated data in the DA system, observing system experiments (OSEs) have been used in the past decades (e.g., Arnold & Dey, 1986; Bouttier & Kelly, 2001; Fujii et al., 2019; Gelaro & Zhu, 2009). In this work, we performed an OSE to evaluate the impact of atmospheric and oceanic data using a coupled regional ocean–atmosphere ensemble model DA system. DA experiments are implemented for the Arabian Sea monsoon onset event in 2023, which also coincides with the passage of the tropical cyclone Biparjoy. This provides us with a unique opportunity to assess air–sea interactions in coupled DA experiments on top of previous studies in the Arabian Sea region during monsoon events (Browne et al., 2019; de Rosnay et al., 2022). In the OSE, we found that when both oceanic and atmospheric data are assimilated, the model skill in forecasting ocean–atmosphere state is improved compared to experiments that assimilate either oceanic or atmospheric data. This indicates that the coupled system provides more balanced initial conditions that can improve the ocean–atmosphere state forecasts. However, we found that assimilating only atmospheric data improves both ocean and atmosphere state forecasts, whereas assimilating only oceanic data improves ocean state forecasts but degrades atmospheric state forecasts, when compared with the free run (coupled model simulation without assimilating any data). We further investigated this counterintuitive model performance, and found this is due to the potential misrepresentation of air–sea exchanges when only oceanic data is assimilated. By comparing DA experiments with and without assimilating atmospheric data, we found that when atmospheric data are not assimilated, forecast errors in the cyclone path increase (i.e., greater offset from the observed cyclone track). Then, assimilating the sea surface temperature (SST) leads to a warmer SST below the misplaced cyclone, resulting in an increased cyclone intensity and deteriorated forecast of the atmospheric state.

In a coupled DA system, the assimilated data from one component can impact the other component through model integration (Laloyaux et al., 2016; Penny et al., 2017). This also suggests that errors in one component can

influence the other component and result in a positive feedback of error growth. In this case study, we hypothesize that the degradation of skill when only oceanic data are assimilated is a general potential failure mode due to the non-linear interactions between ocean and atmosphere. Our OSEs demonstrate the importance of this feedback in situations where atmospheric data are sparse or unavailable (Cardinali, 2013; Geer, 2021; Wang et al., 2022), especially for high-impact atmospheric events such as tropical cyclones, which are becoming more frequent and intense in the northern part of the Indian Ocean.

The rest of the manuscript is organized as follows. We first introduce the coupled ensemble DA system and its implementation in Section 2. The validation of the DA experiments against the data is presented in Section 3. The air–sea exchanges from the comparison of different DA experiments in the OSE are discussed in Section 4. The final section outlines the main findings and concludes this work.

2. Implementation

2.1. The Data Assimilation Framework

We use the SKRIPS coupled model as the forward model and the ensemble adjustment Kalman filter (EAKF) from DART (J. Anderson et al., 2009) to assimilate various oceanic and atmospheric data. Ocean data including satellite-derived along-track sea surface height (SSH), gridded SST, and in situ temperature and salinity profiles were assimilated using the DART–MITgcm interface (Gopalakrishnan et al., 2019; Hoteit et al., 2013, 2015; Sanikommu et al., 2020; Toye et al., 2017). The atmospheric data assimilated are from the National Centers for Environmental Prediction (NCEP) automated data processing (ADP) upper air and surface observations (referred to as PREPBUFR type observations) that include land surface, marine surface, radiosonde, pilot-balloon, aircraft, and satellite data. These atmospheric data are assimilated using the DART–WRF interface (El Gharamti et al., 2025). Because the ocean has much more inertia and evolves more slowly than the atmosphere, we use different time intervals to assimilate oceanic and atmospheric data. We used a 6-hr interval for assimilating atmospheric data and a 3-day interval for assimilating oceanic data. The design of the coupled DA system reflects the different characteristic time scales of the atmosphere and ocean. The 6-hr assimilation cycle for the atmosphere and 3-day assimilation cycle for the ocean are compromises between the computational cost for the EAKF and temporal sampling of the observational data, based on previous DA experiments (El Gharamti et al., 2025; Sanikommu et al., 2025).

In each DA experiment for the coupled system, we initialize both model components, run the coupled model for 6 hr, stop the simulation and assimilate the atmospheric data using the DART–WRF interface, and then restart the model using the atmospheric analyses for next 6 hr. The coupled system will then run and stop every 6 hr for 3 days. Next, we will assimilate the oceanic observations using the DART–MITgcm interface after assimilating the atmospheric data. Once both oceanic and atmospheric data are assimilated, the next coupled DA loop will restart, initialized using the oceanic and atmospheric analyses. The generation of the ocean and atmosphere initial ensembles is set up using the DART–MITgcm and DART–WRF interfaces, which will be further discussed in Section 2.2. The schematic diagram showing the workflow of the regional coupled model DA framework is illustrated in Figure 1. To automate the scripts in the regional coupled DART–SKRIPS framework, we use the ROCOTO workflow management system (Harrop et al., 2017).

The DA schemes used in this work follow our previous experiments (Sanikommu et al., 2020) using DART. In the forecast step, each model ensemble member is integrated forward in time from the last analysis step; then in the analysis step, the forecast ensemble members are adjusted by the incoming data using the EAKF. More details of the EAKF used in the present work can be found in J. L. Anderson (2001) and Toye et al. (2017). Although the ocean and atmosphere models are coupled throughout the experiments, the atmospheric data and oceanic data are assimilated separately by DART–WRF and DART–MITgcm interfaces. This is similar to other weakly coupled DA systems in the literature (e.g., Browne et al., 2019; Zhang et al., 2020).

The SKRIPS model (Sun et al., 2019) is used as the forward model in the coupled model simulation, where the oceanic model component is the MIT general circulation model (MITgcm, Marshall et al., 1997) and the atmospheric model component is the Weather Research and Forecasting (WRF) model (Skamarock et al., 2019). The Earth System Modeling Framework (ESMF, Hill et al., 2004) and the National United Operational Prediction Capability (NUOPC) layer are used to handle the coupling between MITgcm and WRF. The coupled model is also described in the schematic diagram shown in Figure 1. The coupling interval between MITgcm and WRF is

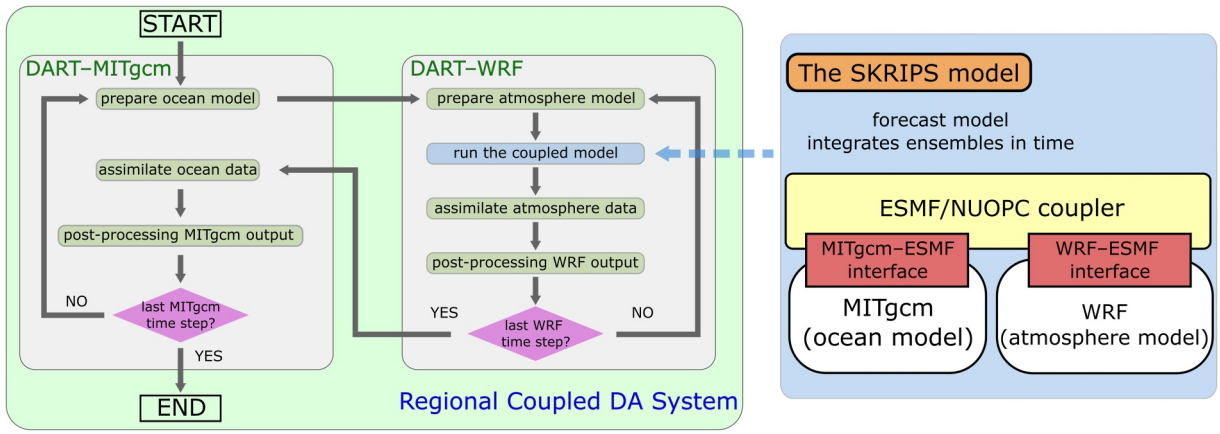


Figure 1. The schematic description of the DART–SKRIPS DA system. The left panel shows the workflow of the coupled DA system. The assimilation of oceanic and atmospheric data are processed separately in DART–SKRIPS for the weakly coupled DA system. The atmospheric data are assimilated every 6 hr before assimilating the oceanic data every 3 days. The right panel shows the structure of the forward model SKRIPS: the yellow block indicates the ESMF coupler; the white blocks are the MITgcm and WRF models; the red blocks are the interfaces between ESMF and the models.

2 min. In the coupling process, MITgcm sends SST and ocean surface velocity to WRF; WRF sends air–sea flux and surface atmospheric fields to MITgcm, including (a) net surface longwave and shortwave radiative fluxes, (b) surface latent and sensible heat fluxes, (c) 10-m wind speed, (d) precipitation, and (e) evaporation. The MITgcm model uses these surface atmospheric variables to prescribe surface forcing, including (a) total net surface heat flux, (b) surface wind stress, and (c) freshwater flux. The total net surface heat flux is computed by adding surface latent heat flux, sensible heat flux, net shortwave radiation flux, and net longwave radiation flux. MITgcm uses the net surface heat fluxes from WRF to ensure that the heat fluxes are consistent in both models (Sun et al., 2019). The surface latent and sensible heat fluxes are computed using the COARE 3.0 bulk algorithm in WRF (Fairall et al., 2003).

2.2. Experimental Design

The aim of the DA experiments is to assess the performance of coupled DA system implemented to understand the air–sea interactions. To this end, we performed a series of 50-member ensemble DA experiments from 07 June 2023 to 07 July 2023, covering the onset of the Indian Ocean monsoon. The OSE is performed using the same setups but with different combinations of data:

1. **CPL.all** assimilates both oceanic and atmospheric data;
2. **CPL.ocn** assimilates only oceanic data;
3. **CPL.atm** assimilates only atmospheric data;
4. **CPL.free** does not assimilate any data.

CPL.free serves as a benchmark to highlight the added value of the coupled DA experiments. The coupled DA experiments: CPL.all, CPL.ocn, and CPL.atm are used to evaluate the effect of different data on the ocean–atmosphere state forecasts.

For coupled model experiments, the ocean model is nested in the Hybrid Coordinate Ocean Model (HYCOM) 1/12° daily global analysis that uses Navy Coastal Ocean Data Assimilation (NCODA), known as the HYCOM Global Ocean Forecast System, Version 3.1, (HYCOM-GOFS3.1 hereinafter, HYCOM) from Chassignet et al. (2007); the atmosphere model is nested in the fifth generation of European Centre for Medium-Range Weather Forecasts global atmospheric reanalysis, known as ERA5 reanalysis (ECMWF, 2017; Hersbach et al., 2020). The SKRIPS model domain extends from 5.24°S to 30.6°N and from 30°E to 91.44°E, covering the Arabian Sea, the Red Sea, the Arabian Gulf, and part of the Bay of Bengal. The horizontal grid resolution is 0.08° for the ocean model and 0.16° for the atmosphere model. There are 56 vertical levels in the ocean model and 50 vertical levels in the atmosphere model (top pressure is 15 hPa). The selection of WRF physics options is based on our previous experiment for Cyclone Mekunu that also occurred in the Arabian Sea region (Sun et al., 2023). The Morrison 2-moment scheme (Morrison et al., 2009) is used to resolve the microphysics; the updated version of the

Table 1
MITgcm Model Physics Parameterizations in the Present Study

Horizontal Viscosity	Vertical Mixing	Horizontal Diffusion
Simple Harmonic (30 m^2/s)	KPP	Implicit Diffusion
Simple Biharmonic (10^7 m^4/s)	PP81	Explicit Diffusion (100 m^2/s)
SMAGLEITH-Harmonic (30 m^2/s),	MY82	GMREDI-clipping (100 m^2/s)
Smag Coeff 2.5, and Leith Coeff 1.85	GGL90	GMREDI-dm95 (100 m^2/s)
		GMREDI-ldd92 (100 m^2/s)

Kain–Fritsch convection scheme (Kain, 2004) is used for cumulus parameterization; the Mellor–Yamada–Nakanishi–Niino 2.5-order closure scheme (Nakanishi & Niino, 2004, 2009) is used for the Planetary Boundary Layer (PBL) and the surface layer; the Rapid Radiation Transfer Model for GCMs (RRTMG, Iacono et al., 2008) is used for longwave and shortwave radiation transfer through the atmosphere; the Noah land-surface model is used for the land-surface processes (Tewari et al., 2004).

For the oceanic simulations in all DA experiments, we use various physical parameterization schemes to account for the effects of unresolved scales of motion as proposed by Sanikommu et al. (2020), summarized in Table 1. Three different categories of model physics are perturbed in the ensemble DA experiments: horizontal viscosity (Griffies & Hallberg, 2000; Holland, 1978; Leith, 1996; Smagorinsky et al., 1993), vertical mixing (Gaspar et al., 1990; W. G. Large et al., 1994; Mellor & Yamada, 1982; Pacanowski & Philander, 1981), and horizontal diffusion (Cox, 1987; Danabasoglu & McWilliams, 1995; Gent & McWilliams, 1990; Gent et al., 1995; W. Large et al., 1997; Redi, 1982). In MITgcm, the initial conditions are obtained from a spin-up run of 10-year MITgcm simulation from 2008 to 2018 using HYCOM-GOFS3.0, by randomly selecting 50 ocean states corresponding to ±15 days from the OSE initial time (June 7). The initial ensembles are sampled at 0000 UTC from the 10-year MITgcm model spin-up simulation. In WRF, the perturbations for initial and lateral boundary conditions are generated from the WRF three-dimensional variational DA (WRF-3DVAR) system using the National Meteorological Center (NMC) method (Parrish & Derber, 1992).

2.3. Data Used in Assimilation

In the ocean component (MITgcm), we assimilate the Operational Sea Surface Temperature and Ice Analysis (OSTIA) SST data (Donlon et al., 2012) from the Copernicus Marine Environment Monitoring Service (CMEMS), the quality controlled in situ temperature and salinity profiles from all types of ocean profiling instruments in EN4 data set (Good et al., 2013; Ingleby & Huddleston, 2007) from the UK Met Office Hadley Centre, and the along-track satellite altimeter SSH from the Radar Altimetry Database System (RADS, http://rads.tudelft.nl/rads/index.shtml, Naeije et al., 2000). The assumed prior error variances for SST and in situ temperature and salinity profiles are consistent with the representational errors of these data.

The OSTIA SST product is assimilated, and SST uncertainties are included in the assumed observational error covariance used in this case study. To avoid duplication of SST data in each model grid, the OSTIA SST data on a $0.05^\circ \times 0.05^\circ$ grid are interpolated onto a $0.25^\circ \times 0.25^\circ$ grid (every five grid points) before the assimilation. The daily gridded OSTIA SST data was averaged over a 3-day window (±1.5 days from the analysis time), and the in situ temperature and salinity profiles were also sampled within the 3-day assimilation window. We use a 3-day interval to assimilate ocean data following our previous data assimilation experiments using ocean-only models (Sanikommu et al., 2020). The SSH from the RADS database is processed with reference to mean dynamic topography DTU17MDT (Knudsen et al., 2021), and were sampled at observation locations within the 3-day assimilation window. The SSHs were assimilated by assuming a spatially and temporally uniform error of 0.05 m. Please refer to Gopalakrishnan et al. (2013, 2019) for further details about SSH processing. A Gaspari–Cohn localization cutoff radius of 300 km was imposed to localize the impact of data in the horizontal direction (no vertical localization is used), mitigating any spurious long-distance correlations (Sanikommu et al., 2020).

In the atmosphere component (WRF), we assimilate the PREPBUFR (NCEP, 2008) land surface, marine surface, radiosonde, pilot-balloon, aircraft, and satellite data. The observation error variance for the PREPBUFR data is determined by the instrument error. The localization cutoff radius of 1,200 km was used for atmospheric data in the horizontal direction. Since the top height in the model is much lower than the horizontal scale of the Earth, the vertical localization radius is defined as 700 hPa, which is comparable to the values used in other DA experiments (Noh et al., 2025; Raeder et al., 2012). The errors associated with these observations are assumed to be uncorrelated, so the observational error covariance matrix is diagonal for both the oceanic and atmospheric data. For the atmospheric state, to avoid potential issues with the ensemble variability, we used the adaptive inflation algorithm proposed in El Gharamti (2018) to mitigate the underestimation of the ensemble spread. No inflation is applied to the oceanic state because its ensemble spread is controlled by the atmosphere (Sanikommu et al., 2020; Sun et al., 2024).

3. Evaluation of Forecast Errors

To validate the ocean–atmosphere state forecasts, we first compute the root-mean-square errors (RMSEs) between the background forecasts and the assimilated data. To further compare the RMSEs, we use the Brier skill score (BSS, Von Storch & Zwiers, 2001) with modifications that simplify the comparison of positive and negative skill scores (Winterfeldt et al., 2011):

$$\mathrm{BSS} = \begin{cases} 1 - \sigma_F^2 \sigma_R^{-2} & \text{if } \sigma_F^2 \le \sigma_R^2, \\ \sigma_R^2 \sigma_F^{-2} - 1 & \text{if } \sigma_F^2 > \sigma_R^2, \end{cases} \tag{1}$$

where σ_F^2 and σ_R^2 are the mean squared error (MSE) of the "forecast" and "reference," respectively. According to Equation 1, positive BSS means a more skillful forecast than the reference, whereas negative BSS means a less skillful forecast than the reference. In addition, the Wilcoxon signed-rank test (Wilks, 2011) is used to determine if the error differences are statistically significant at the 0.05 level, which has been used in other DA experiments to evaluate the forecast performance (Heng et al., 2020; Samrat et al., 2025). It is noted that we are not performing a "true forecast" using forecasted atmospheric and oceanic fields in this study. Our "forecasts" are "hindcasts" that use reanalysis boundary conditions and forcing, isolating the effects of the assimilation-adjusted initial conditions on the model skill in OSEs with combinations of ocean and atmospheric data. The main goal is to test the effects of model analysis in forecasting the ocean and atmosphere state, as analysis fields may not guarantee a good forecast. We thus use "forecast" throughout our manuscript for consistency reasons.

3.1. Oceanic State

The RMSEs of the EAKF ensemble mean ocean forecasts are presented in Figure 2. We present the temporal evolution of the RMSEs of SST, SSH, and in situ temperature and salinity profiles from all the DA experiments. It can be seen that when no data are assimilated (CPL.free), the RMSEs are generally larger than the other experiments, and hence we use the errors in CPL.free as the reference to evaluate the relative forecast performance of the other experiments, summarized in Figure 3. For SST, SSH, and in situ temperature, the ocean state forecast errors in CPL.ocn, CPL.atm, and CPL.all decrease relative to CPL.free, with CPL.all showing the lowest RMSEs. This indicates that assimilating either oceanic or atmospheric data or both data can improve the ocean state forecast. Assimilating the oceanic data reduces the forecast error by 30.9%–69.9%; assimilating the atmospheric data reduces the forecast error by 6%–24.8%. For in situ salinity, the RMSEs in CPL.all are only 11.3% smaller than CPL.free. We hypothesize that this is because the forecast error (0.22 PSU, in CPL.free without assimilating any data) is already smaller than the assumed observation error (0.30 PSU) in the assimilation. When examining the differences between CPL.all and CPL.ocn, we found that assimilating the atmospheric data further improves the ensemble forecast by 8.1%–20.9%, except for the SSH in the Red Sea region. This indicates that the atmospheric observations can positively impact the ocean forecasts in the coupled system. We will further discuss the impact of the atmospheric data on the ocean state forecasts in Section 4.

The differences between the temperature and salinity profiles obtained from the DA experiments against the in situ observations are shown in Figures 4 and 5. The RMSEs of the daily temperature and salinity profiles at the end of each assimilation cycle are averaged and then plotted to demonstrate the temporal evolution of forecast

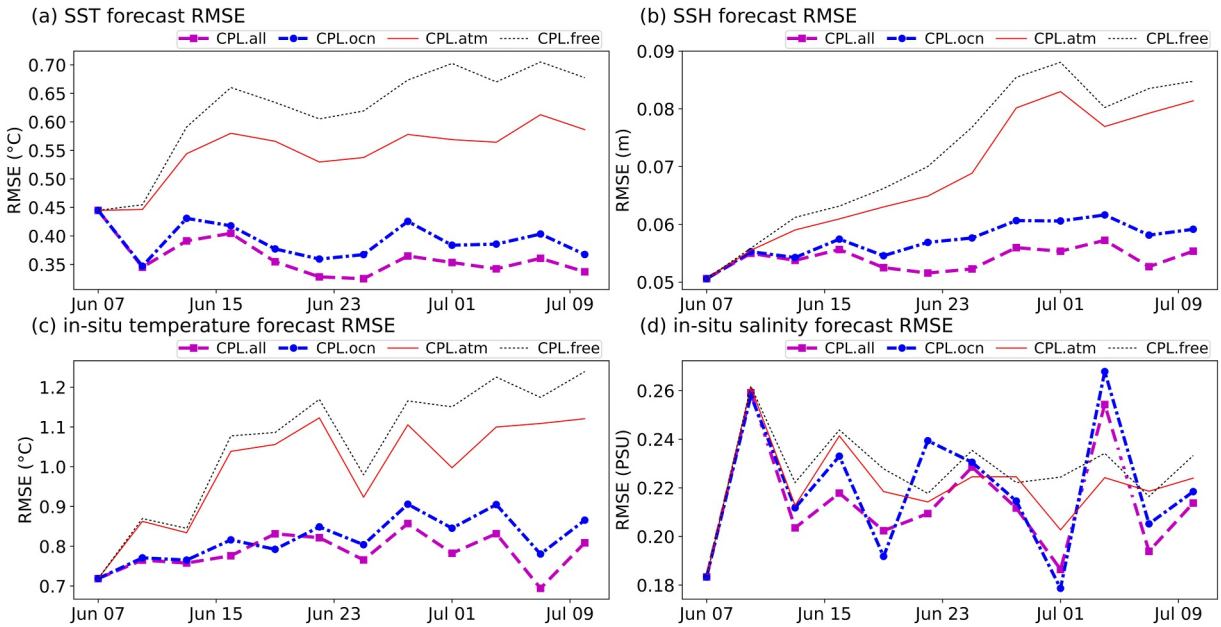


Figure 2. Forecast errors of the oceanic state from the ensemble DA experiments in comparison with assimilated data. Panel (a) shows the RMSEs of the ensemble mean SST; Panel (b) shows the RMSEs of the ensemble mean SSH; Panels (c) and (d) show the RMSEs of the ocean temperature and salinity profiles, respectively. The RMSEs are averaged over the entire ocean model domain and are computed for the forecasts at the end of each 3-day ocean assimilation cycle.

errors. In CPL.all, the largest errors for temperature are found between 0 and 100 m within the ocean boundary layer. Compared with CPL.all, the RMSEs are slightly larger in CPL.ocn (by about 0.2°C) throughout the experiments, especially 15 days (June 22) after the initial time (June 07). This indicates better ocean forecasts above 100 m depth after assimilating the atmospheric observations. The temperature RMSEs change shown in Figure 4b is less than Figure 4c, indicating atmospheric data have much less impact than oceanic data. For the salinity RMSEs in Figure 5, we found larger RMSEs on June 10, June 22, and July 04 in CPL.all. These are primarily due to errors in the salinity changes induced by the Red Sea Outflow Water (RSOW, Bower et al., 2000; Yao et al., 2014) that need to be addressed in our future work. The forecast error difference in salinity between CPL.all and CPL.ocn is only 5.1% (shown in Figure 3) and is not statistically significant, but CPL.all still shows better skill than CPL.free after assimilating the salinity observations.

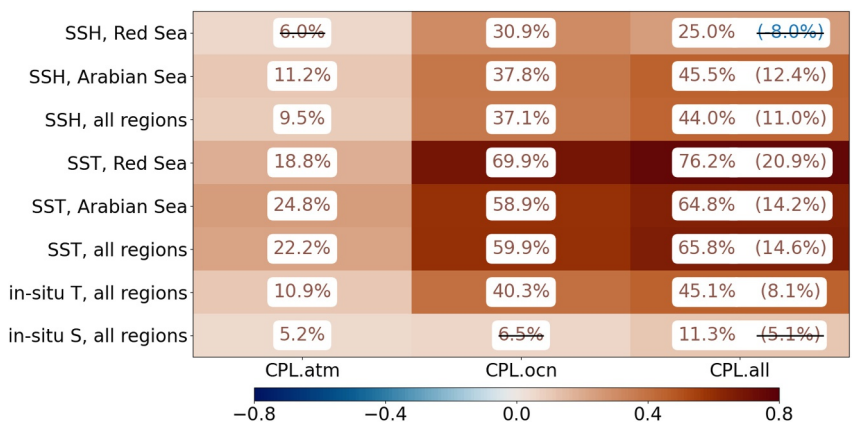


Figure 3. The Brier Skill Scores (BSSs) of the ocean state obtained from the coupled DA experiments compared with CPL.free. The numbers in parentheses are the BSSs of CPL.all relative to CPL.ocn. If the number is crossed out, it means that the difference is not significant at the 0.05 level determined using the Wilcoxon signed-rank test (sample size = 11 for the 3-day ocean assimilation cycle throughout the DA experiment).

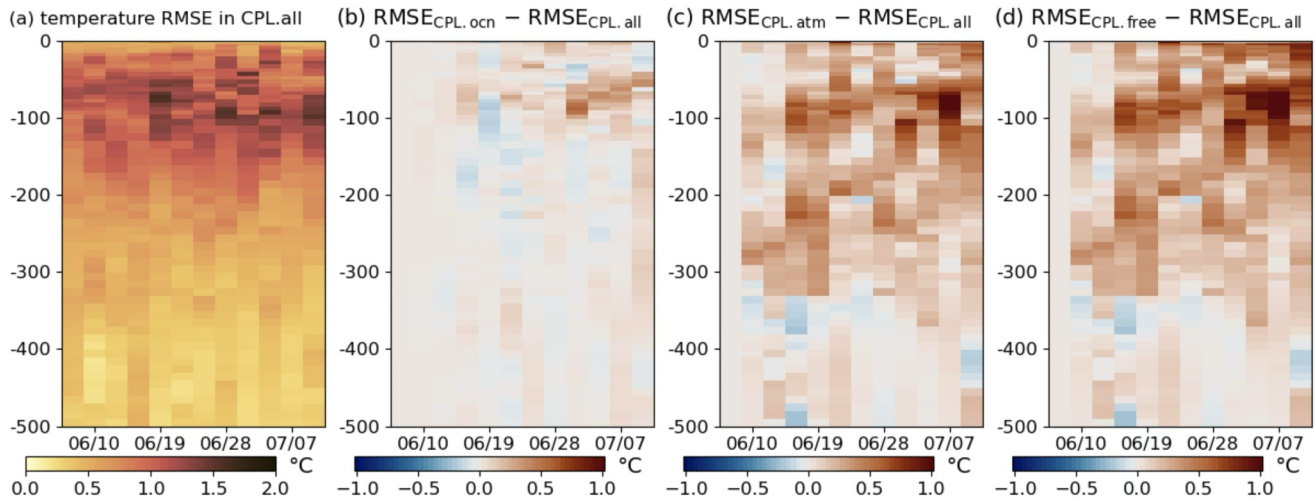


Figure 4. Profiles of ocean temperature RMSEs obtained from the DA experiments in comparison with in situ data. Panel (a) shows the averaged temperature RMSEs from all profiles in CPL.all; Panels (b–d) are the RMSEs obtained from CPL.ocn, CPL.atm, and CPL.free, respectively, minus the RMSEs from CPL.all. Positive differences indicate that the experiment has larger RMSEs than CPL.all. The RMSEs are averaged for all the profiles in EN4 data set assimilated in the CPL.all at the end of each 3-day ocean assimilation cycle.

3.2. Atmospheric State

To evaluate the forecasts of atmosphere state in the coupled DA experiment, we present the temporal evolution of 2-m air temperature and 10-m zonal and meridional wind speeds in Figure 6. It can be seen that when atmospheric observations are assimilated in CPL.all or CPL.atm, the RMSEs decrease compared to CPL.free, suggesting that assimilating atmospheric data can improve the atmospheric forecast. For the 2-m air temperature, the RMSEs in CPL.ocn are smaller than CPL.atm, indicating that, in this case, assimilating oceanic data contributes to improved 2-m temperature forecasts when atmospheric data are limited. In the zonal and meridional wind speed comparison, we find that (a) the RMSEs obtained for CPL.all and CPL.atm are comparable; and (b) the RMSE obtained for CPL.ocn is larger than other experiments.

Because the RMSEs are close between the CPL.all and CPL.atm, we evaluate the BSSs and summarize the results in Figure 7 by category of the assimilated atmospheric data. The forecast skill is better in CPL.all and CPL.atm

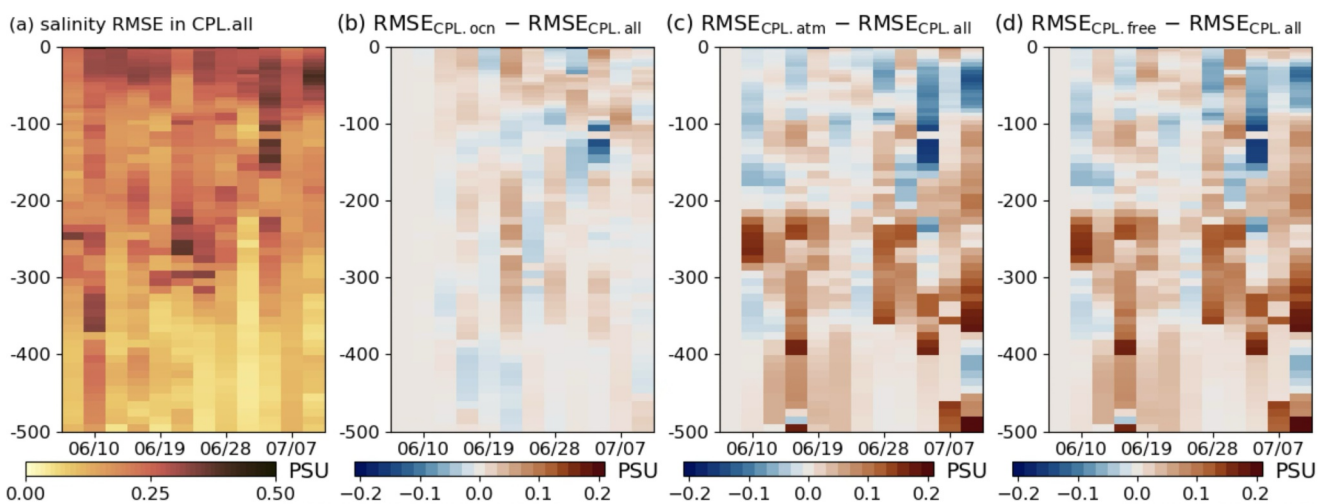


Figure 5. Profiles of ocean salinity RMSEs obtained from the DA experiments in comparison with in situ data. Panel (a) shows the averaged salinity RMSEs from all profiles in CPL.all; Panels (b–d) are the RMSEs obtained from CPL.ocn, CPL.atm, and CPL.free, respectively, minus the RMSE from CPL.all. Positive differences indicate that the experiment has larger RMSEs than CPL.all. The RMSEs are averaged for all the profiles in EN4 data set assimilated in the CPL.all at the end of each 3-day ocean assimilation cycle.

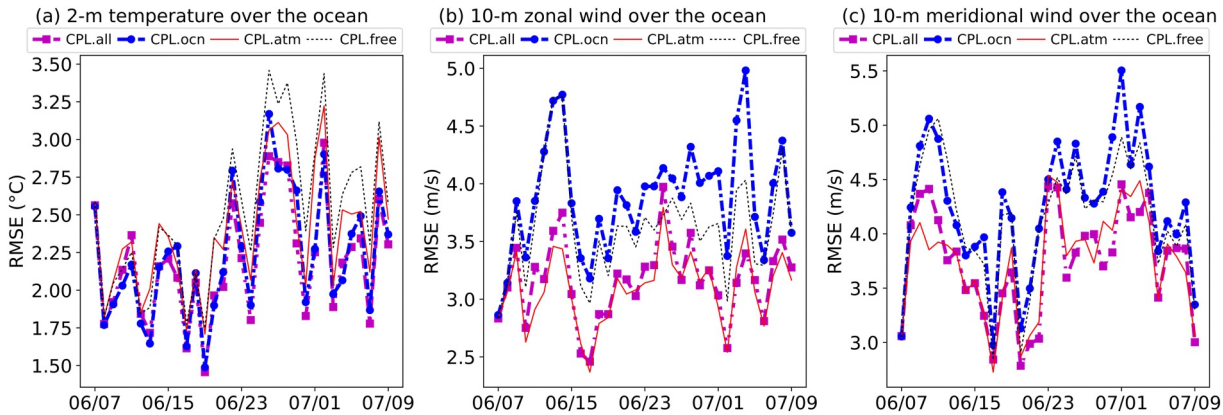


Figure 6. Six hour lead-time forecast errors of the atmospheric state from the ensemble DA experiments in comparison with assimilated data. Panels (a–c) are the RMSEs of ensemble mean 2-m air temperature, 10-m zonal wind speed, and 10-m meridional wind speed, respectively. The RMSEs are the average between the atmospheric forecasts and the PREPBUFR atmospheric data within the ocean domain, and are computed at the end of each 6-hr atmosphere assimilation cycle. Only the RMSEs at 0000 UTC obtained in the DA experiments are shown.

than in CPL.free for all atmospheric variables. The main difference between CPL.all and CPL.atm is for 2-m air temperature (16.4%) when SST is assimilated in CPL.all, showing the positive impacts on atmospheric state forecasts by assimilating oceanic data in the coupled DA system. CPL.all also has slightly better forecast skill than CPL.atm for other atmospheric variables, but their differences are not statistically significant for most variables, with the maximum differences between −4.5% and 4.3%. This indicates that oceanic data do not significantly improve the estimates when atmospheric data are already assimilated in this coupled DA case study. However, when atmospheric data are not assimilated, the CPL.ocn forecast errors of atmospheric variables (except for 2-m air temperature) are increased by 4.9%–26.2% when compared with CPL.free. This unexpected negative impact of oceanic data on atmospheric forecasts will be further discussed in Section 4.

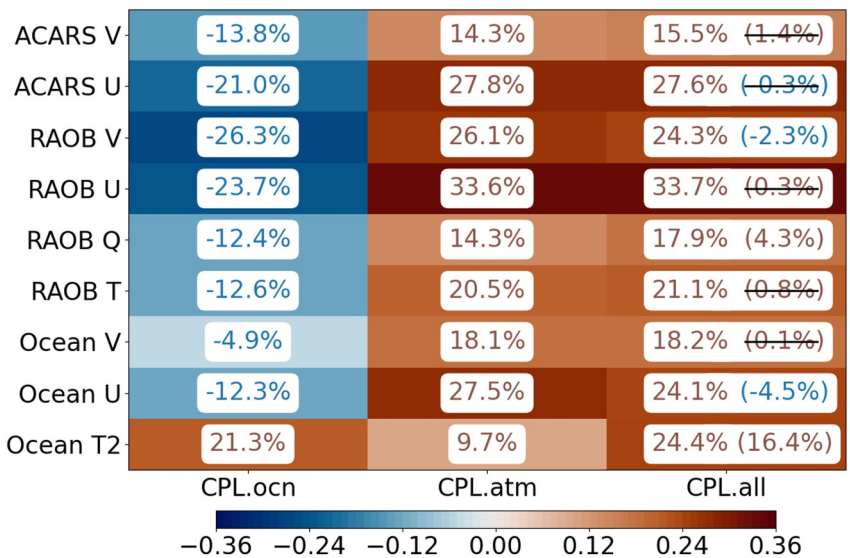


Figure 7. The Brier Skill Scores (BSSs) of the atmospheric state obtained from the coupled DA experiments compared with CPL.free. The numbers in parentheses are the BSSs of CPL.all relative to CPL.ocn. Ocean T2 indicates 2-m air temperature above ocean; Ocean U10 indicates 10-m zonal wind speed above ocean; Ocean V10 indicates 10-m meridional wind speed above ocean; RAOB T indicates radiosonde temperature; RAOB Q indicates radiosonde specific humidity; RAOB U indicates radiosonde zonal wind speed; RAOB V indicates meridional wind speed; ACARS U indicates ACARS zonal wind speed; ACARS V indicates ACARS meridional wind speed. If the number is crossed out, it means that the difference is not significant at the 0.05 level determined using the Wilcoxon signed-rank test (sample size = 132 for the 6-hr atmospheric assimilation cycle throughout the DA experiment). Because the PREPBUFR only contains quality-controlled satellite data at upper levels in the Bay of Bengal region, we do not show the comparison with satellite data.

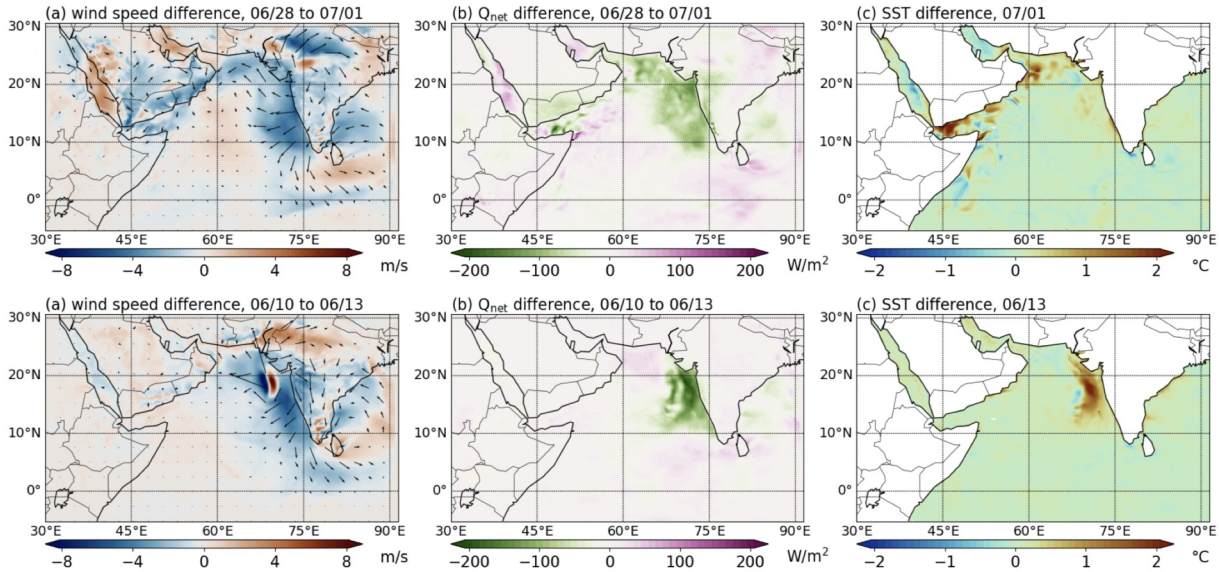


Figure 8. The differences in the 10-m wind speed (3-day averaged), surface heat fluxes Q_{net} (3-day averaged), and SST (snapshot after the 3-day forecast) between CPL.all and CPL.ocn (CPL.all minus CPL.ocn). Positive wind speed indicates CPL.all is more windy; positive Q_{net} indicates CPL.all loses more heat in the ocean; positive SST indicates CPL.all is warmer. Panels (a–c) are these variables obtained between June 10 and 13; Panels (d–f) are between June 28 and July 01. The wind speed and heat fluxes are obtained by averaging the atmosphere forecast every 6 hr over the 3-day assimilation cycle.

4. Discussion

The performance of the coupled DA experiments against the assimilated data has been presented in the previous section. To explore the differences in forecast skill, we examine the air–sea interactions in the estimates that include or exclude the oceanic or atmospheric data.

4.1. Atmospheric Data Impact on Ocean Forecasts

When atmospheric observations are assimilated in CPL.all and CPL.atm, the ocean forecasts are improved compared to CPL.ocn and CPL.free. This shows that atmospheric data have positive impacts on ocean forecasts. Here, we examine the differences between CPL.all and CPL.ocn to further explore the effects of the assimilated atmospheric data. Figure 8 shows their differences in 10-m wind speed, surface heat fluxes Q_{net}, and SST. We selected two snapshots (June 13 and July 01) in the experiments, aiming to illustrate the air–sea exchanges for the 3-day forecasts during and after the cyclone event. Between June 10 and June 13, the atmospheric data assimilated in CPL.all decreases the wind speed in the eastern Arabian Sea near Cyclone Biparjoy. Because cyclone Biparjoy is less intense, the ocean loses less heat. Although the initial SST conditions are similar in CPL.all and CPL.ocn on June 10, after assimilating the oceanic data, the SST is warmer in CPL.all than CPL.ocn after the 3-day forecast, except under Cyclone Biparjoy. Figure 7 indicates that the atmospheric variables in CPL.all are closer to the observations than CPL.ocn, and better representation of atmospheric state leads to better forecasts of SST and other ocean state variables in CPL.all. The other snapshot on July 01 also shows the interactions between ocean and atmosphere components in the coupled DA system. In CPL.all, the wind speed in the eastern Arabian Sea is weaker by 4–8 m/s after assimilating the atmospheric data. During the 3-day forecast from June 28 to July 01, the surface heat fluxes Q_{net} also decreases in this region and lead to warmer SST in CPL.all, which improves the SST forecast skill when compared with the data.

Because the ensemble spread of the atmospheric state can play an important role in the prediction of the ocean state (Sanikommu et al., 2020; Sun et al., 2024), we show the evolution of the ensemble spread of the surface atmospheric variables in the experiments in Figure 9. Although we used inflation for the atmosphere ensembles in CPL.all to increase their variance when assimilating the atmospheric observations, the ensemble spread of the 10-m wind speed in CPL.all is comparable to CPL.ocn during the cyclone event from June 07 to June 19, and gets smaller than CPL.ocn after the cyclone event. Because CPL.all has smaller ensemble spreads for 2-m temperature and 10-m wind speeds when compared with other experiments, the improved ocean–atmosphere forecast skill in

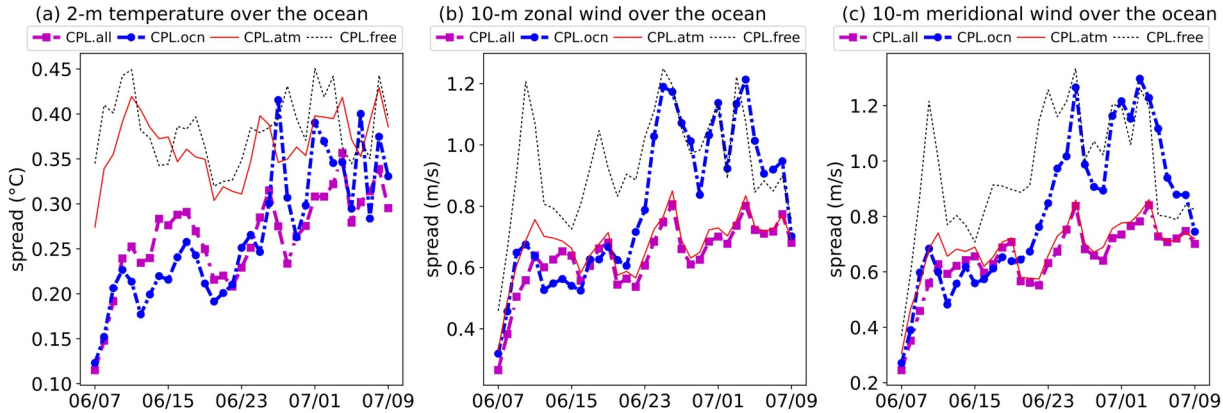


Figure 9. The ensemble spreads of the atmospheric variables in the DA experiments. Panels (a–c) are the spreads of 2-m temperature, 10-m zonal wind speed, and 10-m meridional wind speed, respectively. The ensemble spreads are the average at the location of all the observations in the ocean domain used in Figure 6, and computed at the end of each 6-hr atmosphere assimilation cycle. Only the ensemble spreads at 0000 UTC obtained in the DA experiments are shown.

CPL.all is not gained from increasing the background error covariance using inflation, but from improved representation of the atmospheric state in the coupled system.

4.2. Oceanic Data Impact on Atmospheric Forecasts

We have shown in Figure 7 that the forecast skill of the atmospheric state in CPL.ocn degraded after assimilating oceanic data compared to CPL.free. To understand the impact of oceanic data on atmospheric forecasts, we examined the changes in SST and 10-m wind speeds obtained from these two experiments. We used the same snapshots as Section 4.1 to highlight the impact of oceanic data during the cyclone and after. First, the wind speeds are shown to illustrate the differences in the atmospheric state. The wind speed in CPL.ocn is stronger than that in CPL.free, with the differences shown in Figure 10d, indicating that assimilating the oceanic data increases the intensity of the cyclone on June 13. Figure 10f shows the errors in cyclone path in the DA experiments. Without assimilating the atmospheric data, the errors in the cyclone path for CPL.ocn and CPL.free are about 200 km compared with the IBTrACS data (Knapp et al., 2010). In CPL.free, the tropical cyclone induces surface ocean cooling ("cold-wake") which limits the intensification of the cyclone. However, because of the eastward offset of the cyclone path in CPL.ocn, assimilating the SST leads to a warmer SST (shown in Figure 10f) below

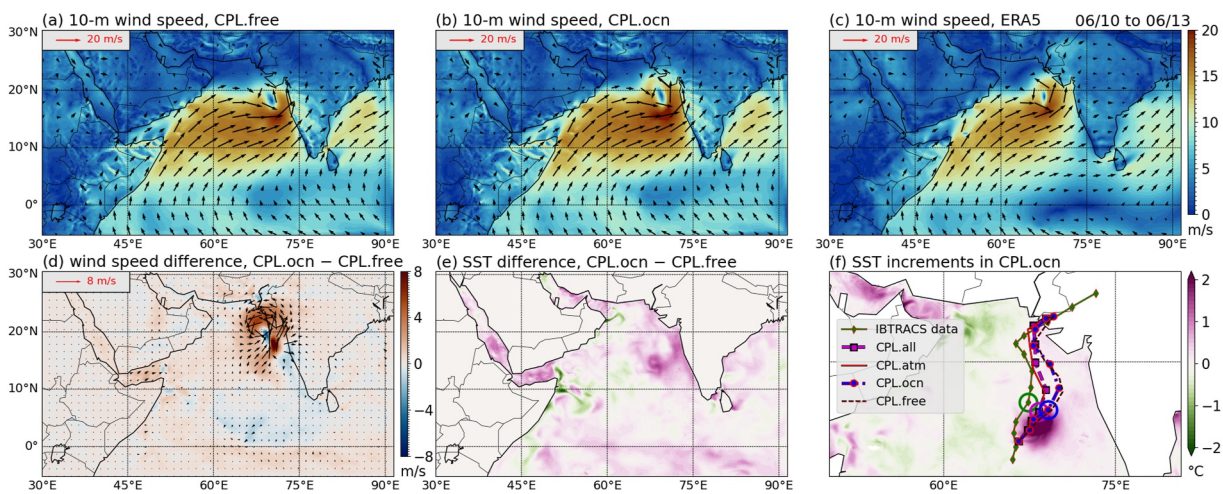


Figure 10. The 10-m wind speed and SST differences for CPL.ocn and CPL.free between June 10 and 13. Panels (a–c) are the 10-m wind speed from CPL.ocn, CPL.free, and ERA5 atmospheric reanalysis. Panels (d–e) are the differences between CPL.ocn and CPL.free (CPL.ocn minus CPL.free) in 10-m wind speed and SST, respectively. Positive wind differences in Panel (d) indicate CPL.ocn is more windy than CPL.free; positive SST differences in Panel (e) indicate CPL.ocn is warmer than CPL.free. Panel (f) is the SST increments in CPL.ocn after assimilating the oceanic data on June 10. The dashed line in Panel (f) indicates the cyclone path from IBTrACS data; the other lines indicate the cyclone paths simulated using DA experiments. The cyclone's locations on June 10 are highlighted.

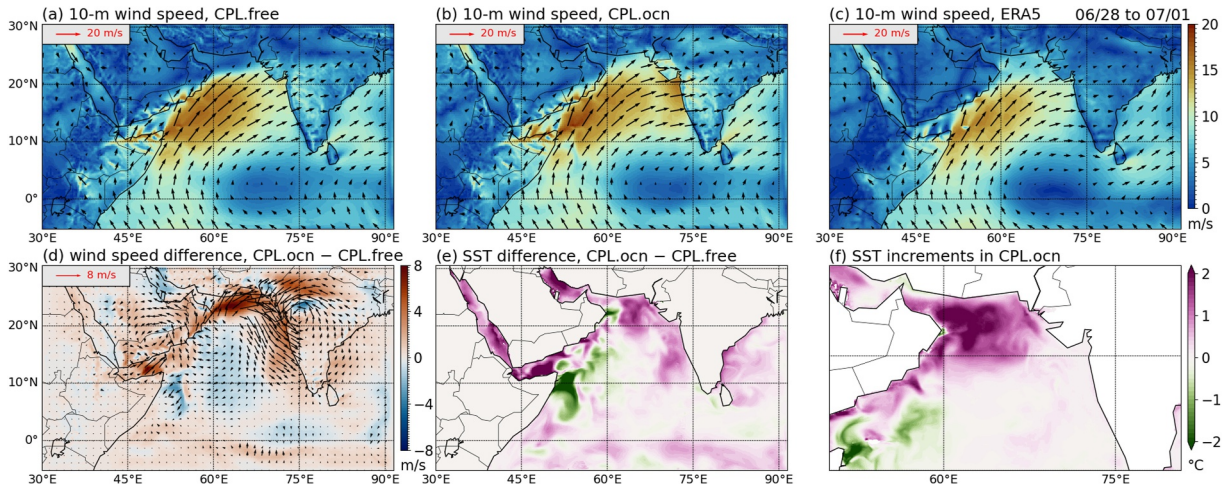


Figure 11. Same as Figure 10, but for the 10-m wind speed and SST differences between June 28 and July 01.

the cyclone for the forecasts, resulting in an increased cyclone intensity. This suggests that, in this particular case, the air–sea exchanges are misrepresented in CPL.ocn when only oceanic data are assimilated. The misrepresentation of air–sea exchanges continues to occur after the cyclone event, shown in Figure 11. For example, on June 28 the SST in the eastern Arabian Sea gets warmer by about 1°C, and generates cyclonic surface wind patterns east of the Arabian Sea that lead to larger RMSEs in the atmospheric state between June 28 and July 01. The cyclonic wind patterns are also documented in our previous SST sensitivity study for the Indian Ocean monsoon (Sun et al., 2026). More snapshots of the SST analyses (initial SST condition), wind speed, and SST forecasts in the DA experiments are detailed in Appendix A to demonstrate the SST and wind speed differences between the two experiments.

The characteristics of the cyclones obtained in the simulations are summarized in Figure 12. After assimilating both oceanic and atmospheric data, the oceanic and atmospheric states are more balanced across the coupled model in CPL.all. Compared with the IBTrACS data, the offset of the cyclone path in CPL.all is smaller than in

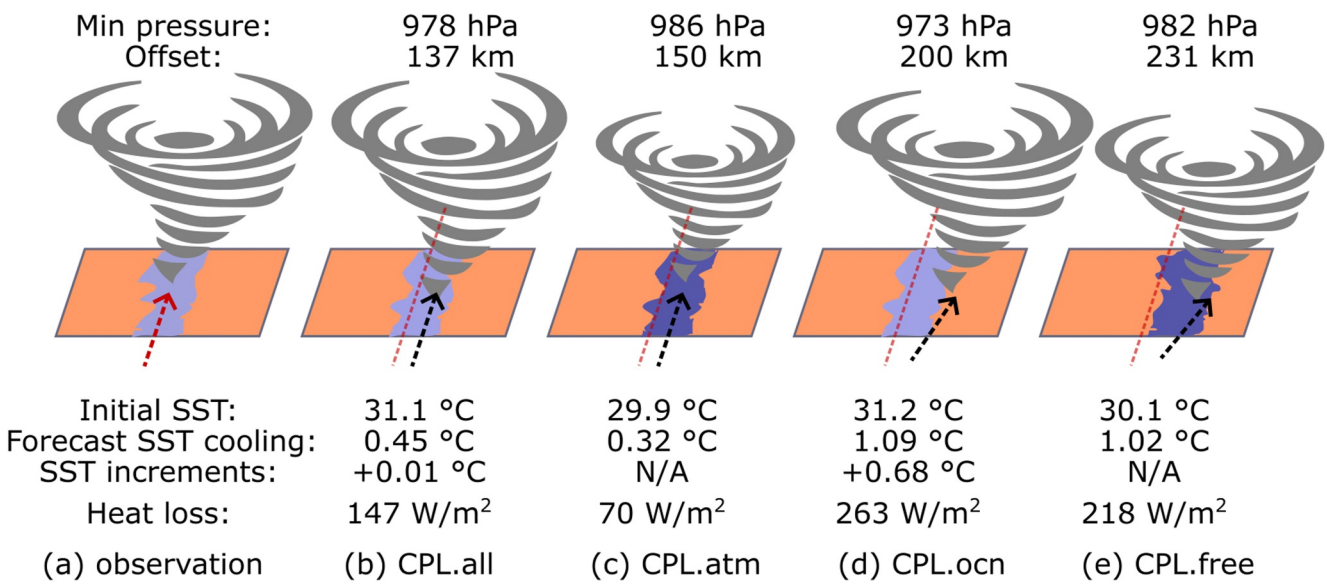


Figure 12. The characteristics of the cyclones on June 10 obtained from all the simulations. The initial SST is the SST below the cyclone on June 10. The SST cooling and heat fluxes are computed between June 10 and 13 along the cyclone track for the region 16N°–20N° and 66E°–72E°. The red dashed lines indicate the movement of the cyclone from IBTrACS data; the black dashed lines indicate the movement of the cyclone in the DA experiments. The offset is the great-circle distance between simulated and observed cyclone centers on June 10.

other experiments. We also examined the SST changes between June 10 and 13 along the cyclone track over the region 16N°–20N° and 66E°–72E°. Again, CPL.all has the smallest forecast errors in SST compared to the observations. This suggests that the forecasts initialized from a more balanced state in CPL.all using the coupled DA system, reduces the misrepresentation of air–sea exchanges exhibited in CPL.ocn. The averaged heat fluxes (Q_{net}) are also calculated for the same region between June 10 and 13. In CPL.ocn the heat losses are about twice as much as CPL.all, indicating that the cyclone gained more heat from the ocean when assimilation of ocean temperature results in a warmer ocean below the misplaced cyclone in CPL.ocn experiment.

This study suggests that the forecasts from a more balanced state in CPL.all using the coupled DA system will reduce the misrepresentation of air–sea exchanges shown in CPL.ocn. In addition, the offset of the cyclone path can be reduced by assimilating atmospheric data, but not by assimilating ocean data alone. The forecasts in CPL.ocn highlight potential strong nonlinearity in coupled DA experiments with strong, localized, and coupled features. Better forward models, initial conditions, and improved DA schemes are still desirable for coupled DA experiments, especially when atmospheric data are limited in space and time, and also during extreme atmospheric events like cyclones.

5. Summary and Conclusions

In this work, we first developed a new regional coupled ocean–atmospheric ensemble DA system for the Northern Indian Ocean region using the SKRIPS coupled model and the DART-EAKF DA scheme. Then, we explored the air–sea interactions in the coupled system using an OSE for the Arabian Sea monsoon onset in 2023. This study period also coincides with the passage of a tropical cyclone Biparjoy, which formed over the east-central Arabian Sea on June 6, and traversed the east Arabian Sea and made landfall in Naliya, India, on June 16.

We found that assimilating both oceanic and atmospheric data in the coupled DA system (CPL.all) improves ocean and atmosphere forecasts, showing lower model–data RMSEs, compared to forecasts from DA experiments of free run (CPL.free), assimilating only atmospheric data (CPL.atm), and assimilating only oceanic data (CPL.ocn). In CPL.all, the oceanic and atmospheric initial conditions are better aligned, leading to improved ocean–atmosphere forecasts. However, compared to the free run (CPL.free), assimilating only atmospheric data (CPL.atm) improves both atmosphere and ocean forecasts, while assimilating only oceanic data (CPL.ocn) improves ocean forecasts but degrades atmospheric forecasts. This poor atmospheric forecast skill for CPL.ocn is due to the misrepresentation of air–sea exchanges, especially during the passage of Cyclone Biparjoy. Although the misrepresentation of air–sea exchanges is due to assimilating the oceanic data, it also indicates the limitations of the coupled forward model in accurately simulating the tropical cyclone and the monsoon.

In this work, we explored the importance of atmospheric and oceanic observations using two extreme cases (CPL.atm and CPL.ocn). Our OSEs demonstrate that, given our metrics, the atmospheric observations are more important for accurately forecasting the oceanic and atmospheric states. Additionally, this work documents a generic failure mode in regional weakly coupled DA experiments when atmospheric observations are sparse or unavailable. This failure is most likely to arise in the presence of highly nonlinear extreme events, like strong tropical cyclones. It also highlights the importance of the forward model and the accurate initial conditions used in the coupled system. In addition, this case study suggests that operational systems should be cautious when running ocean-only DA experiments in cyclone-prone regions.

Future work will involve further investigating the air–sea interactions in the weakly coupled DA system for different time periods, which can help to understand land-sea breeze processes in the Red Sea region and monsoon precipitation. Additional DA experiments to diagnose the forward model discrepancies and to find ways to improve model representation of tropical cyclones are undergoing. Additional satellite data (e.g., surface winds and GPS radio occultation data) and in situ observation data from the ASTraL/EKAMSAT field campaign will also be assimilated in our future experiments.

Appendix A: Evolution of SST and Wind Speed

The snapshots of SST and wind speed are displayed in Figures A1 and A2 to show the evolution of oceanic and atmospheric states in the DA experiments. Two snapshots are selected (i.e., June 10 and June 28) to highlight the impact of the assimilated SST on the atmosphere before and after the cyclone. On June 10, the initial SST is warmer in CPL.ocn after assimilating the data, and thus the cyclone intensity in CPL.ocn is stronger than that in

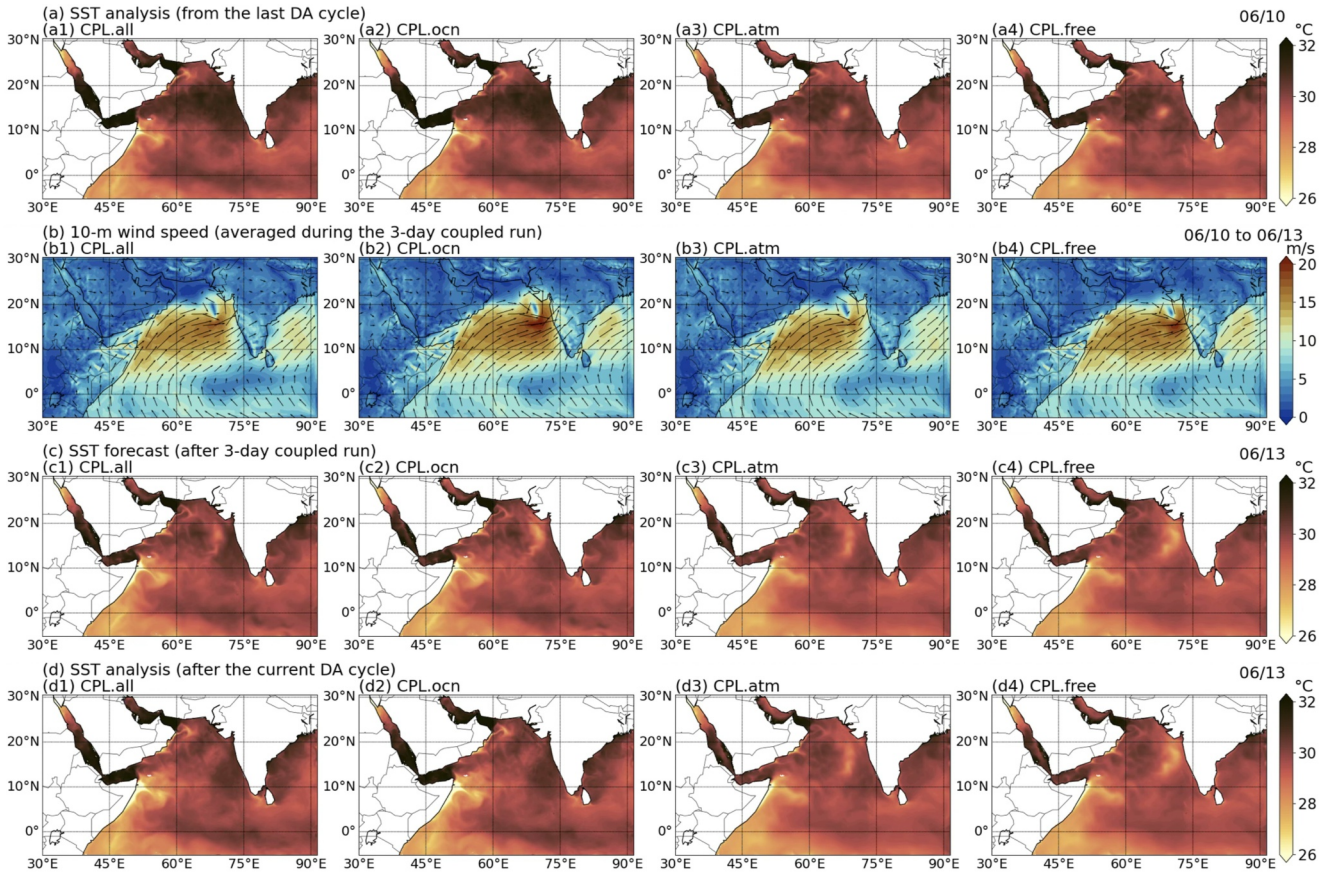


Figure A1. Evolution of SST and wind speed between June 10 and June 13 in CPL.all, CPL.ocn, CPL.atm, and CPL.free. Panels (a1–a4) are the SST analyses on June 10 from the previous DA cycle (also the initial SST condition for the current DA cycle); Panels (b1–b4) are the 10-m wind speeds averaged between June 10 and June 13 in the 3-day forecasts (surface wind forcing); Panels (c1–c4) are the SST forecasts on June 13; Panels (d1–d4) are the SST analyses on June 13 after the 3-day forecasts (also the initial SST condition for the next DA cycle).

CPL.free. The SST cools down by about 2°C after the 3-day simulation in both CPL.ocn and CPL.free, but the SST in CPL.ocn becomes warmer than CPL.free after assimilating oceanic data on June 13, which further increases the cyclone intensity in the 3-day simulation. The SST fields show cyclone induced cold wake in CPL.ocn and CPL.free, but after assimilating the observed SST in CPL.ocn the air–sea exchanges are misrepresented. The misrepresentations are reduced in CPL.all and the RMSEs in wind speed are smaller, and the cyclone intensity is also stronger in CPL.all than CPL.atm after assimilating the observed SST.

On June 28, the SST in CPL.ocn is still warmer than CPL.free after assimilation, shown in Figure A2. The SST is warmer in the northern and eastern Arabian Sea by about 2°C. Because of the warmer SST, there is a cyclonic wind pattern in CPL.ocn (also shown in Figure 11) that affects these regions, which leads to much larger RMSEs in the atmospheric forecasts compared to CPL.free. In addition, the larger RMSEs in wind speed in CPL.ocn also lead to increased RMSEs of the SST forecasts compared to CPL.ocn.

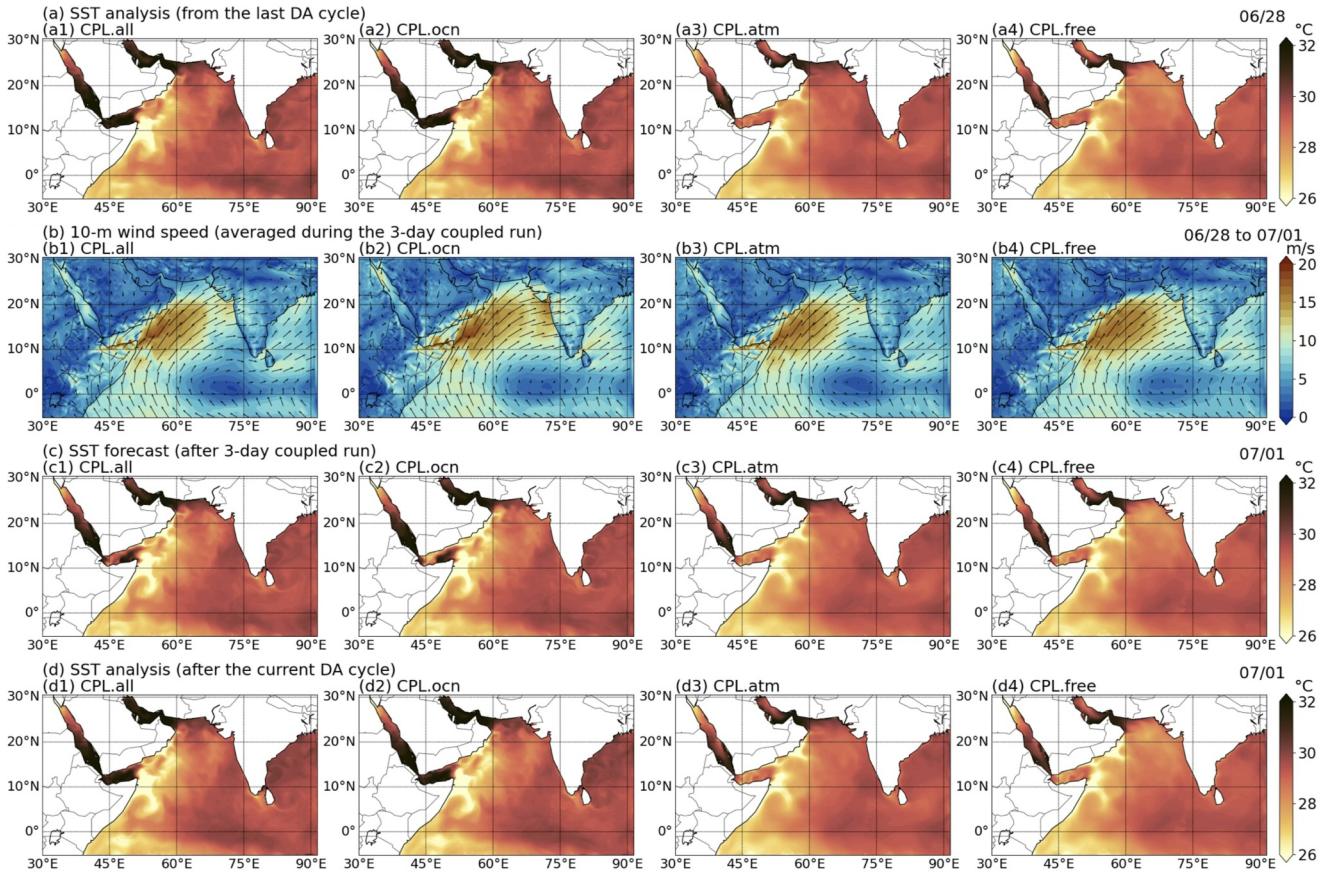


Figure A2. Same as Figure A1, but for June 28–July 01.

Conflict of Interest

The authors declare no conflicts of interest relevant to this study.

Acknowledgments

We gratefully acknowledge the research funding (Grant OSR-2022-NCM-4829.5) from the Climate Change Center at KAUST (King Abdullah University of Science and Technology). We also appreciate the ONR ASTraL research initiative (N00014-23-1-2092). ACS was also supported by NOAA Grant NA18OAR4310405 and KAUST CRG Grant ORA-2021-CRG10-4649.2. BDC and MRM were supported by NOAA Grant NA21OAR4310257, NA18OAR4310403, and NA22OAR4310597. AJM was partly supported by the National Science Foundation (OCE-2022868). GG was supported by ONR funding N000142112726. The DA experiments were performed on KAUST supercomputer SHAHEEN III and we appreciate the computational resources provided by KAUST Supercomputer Laboratory. We gratefully appreciate the support from the Data Assimilation Research Section (DAReS) at NCAR for developing the coupled DA framework.

Availability Statement

The WRF model used for the simulations is described at https://www2.mmm.ucar.edu/wrf/users/download/get_source.html from Skamarock et al. (2019). We obtained the WRF code from https://github.com/wrf-model/WRF for version 4.5.1. The ERA5 data are obtained from the Copernicus Climate Data Store available at Hersbach et al. (2023a, 2023b). The assimilated PREPBUFR data are available at https://doi.org/10.5065/Z83F-N512 from NCEP (2008). The IBTrACS validation data are obtained from Gahtan et al. (2024).

References

Anderson, J., Hoar, T., Raeder, K., Liu, H., Collins, N., Torn, R., & Avellano, A. (2009). The data assimilation research testbed: A community facility. *Bulletin of the American Meteorological Society*, *90*(9), 1283–1296. https://doi.org/10.1175/2009bams2618.1

Anderson, J. L. (2001). An ensemble adjustment Kalman filter for data assimilation. *Monthly Weather Review*, *129*(12), 2884–2903. https://doi.org/10.1175/1520-0493(2001)129<2884:aeakff>2.0.co;2

Arnold, C. P., Jr., & Dey, C. H. (1986). Observing-systems simulation experiments: Past, present, and future. *Bulletin of the American Meteorological Society*, *67*(6), 687–695. https://doi.org/10.1175/1520-0477(1986)067<0687:ossepp>2.0.co;2

Bouttier, F., & Kelly, G. (2001). Observing-system experiments in the ECMWF 4D-Var data assimilation system. *Quarterly Journal of the Royal Meteorological Society*, *127*(574), 1469–1488. https://doi.org/10.1256/smsqj.57418

Bower, A. S., Hunt, H. D., & Price, J. F. (2000). Character and dynamics of the Red Sea and Persian Gulf outflows. *Journal of Geophysical Research*, *105*(C3), 6387–6414. https://doi.org/10.1029/1999jc900297

Browne, P. A., De Rosnay, P., Zuo, H., Bennett, A., & Dawson, A. (2019). Weakly coupled ocean–atmosphere data assimilation in the ECMWF NWP system. *Remote Sensing*, *11*(3), 234. https://doi.org/10.3390/rs11030234

Cardinali, C. (2013). Observation influence diagnostic of a data assimilation system. In *Data assimilation for atmospheric, oceanic and hydrologic applications* (Vol. II, pp. 89–110). Springer.

Chassignet, E. P., Hurlburt, H. E., Smedstad, O. M., Halliwell, G. R., Hogan, P. J., Wallcraft, A. J., et al. (2007). The HYCOM (hybrid coordinate ocean model) data assimilative system. *Journal of Marine Systems*, *65*(1), 60–83. https://doi.org/10.1016/j.jmarsys.2005.09.016

Cox, M. (1987). Isopycnal diffusion in a z-coordinate ocean model. *Ocean Modelling*, *74*, 1–5.

Danabasoglu, G., & McWilliams, J. (1995). Sensitivity of the global ocean circulation to parameterizations of mesoscale tracer transports. *Journal of Climate*, *8*(12), 2967–2987. https://doi.org/10.1175/1520-0442(1995)008<2967:sotgoc>2.0.co;2

de Rosnay, P., Browne, P., de Boisséson, E., Fairbairn, D., Hirahara, Y., Ochi, K., et al. (2022). Coupled data assimilation at ECMWF: Current status, challenges and future developments. *Quarterly Journal of the Royal Meteorological Society*, *148*(747), 2672–2702. https://doi.org/10.1002/qj.4330

Donlon, C. J., Martin, M., Stark, J., Roberts-Jones, J., Fiedler, E., & Wimmer, W. (2012). The operational sea surface temperature and sea ice analysis (OSTIA) system. *Remote Sensing of Environment*, *116*, 140–158. https://doi.org/10.1016/j.rse.2010.10.017

ECMWF. (2017). *Era5 data documentation* (Tech. Rep.). European Center for Medium-Range Weather Forecasts.

Edwards, C. A., Moore, A. M., Hoteit, I., & Cornuelle, B. D. (2015). Regional ocean data assimilation. In C. Carlson & S. Giovannoni (Eds.), *Annual review of marine science* (Vol. 7(No. (1), pp. 21–42). https://doi.org/10.1146/annurev-marine-010814-015821

El Gharamti, M. (2018). Enhanced adaptive inflation algorithm for ensemble filters. *Monthly Weather Review*, *146*(2), 623–640. https://doi.org/10.1175/mwr-d-17-0187.1

El Gharamti, M., Kershaw, H., Raeder, K., Raczka, B., Johnson, B., Smith, M., & Gaubert, B. (2025). The data assimilation research testbed: A robust, scalable software facility with groundbreaking capabilities for model-data integration. *Bulletin of the American Meteorological Society, BAMS–D*.

Fairall, C., Bradley, E. F., Hare, J., Grachev, A., & Edson, J. (2003). Bulk parameterization of air–sea fluxes: Updates and verification for the COARE algorithm. *Journal of Climate*, *16*(4), 571–591. https://doi.org/10.1175/1520-0442(2003)016<0571:bpoasf>2.0.co;2

Flato, G. M. (2011). Earth system models: An overview. *Wiley Interdisciplinary Reviews: Climate Change*, *2*(6), 783–800. https://doi.org/10.1002/wcc.148

Fowler, A. M., & Lawless, A. S. (2016). An idealized study of coupled atmosphere–ocean 4D-Var in the presence of model error. *Monthly Weather Review*, *144*(10), 4007–4030. https://doi.org/10.1175/mwr-d-15-0420.1

Frolov, S., Bishop, C. H., Holt, T., Cummings, J., & Kuhl, D. (2016). Facilitating strongly coupled ocean–atmosphere data assimilation with an interface solver. *Monthly Weather Review*, *144*(1), 3–20. https://doi.org/10.1175/mwr-d-15-0041.1

Fujii, Y., Ishibashi, T., Yasuda, T., Takaya, Y., Kobayashi, C., & Ishikawa, I. (2021). Improvements in tropical precipitation and sea surface air temperature fields in a coupled atmosphere–ocean data assimilation system. *Quarterly Journal of the Royal Meteorological Society*, *147*(735), 1317–1343. https://doi.org/10.1002/qj.3973

Fujii, Y., Rémy, E., Zuo, H., Oke, P., Halliwell, G., Gasparin, F., et al. (2019). Observing system evaluation based on ocean data assimilation and prediction systems: On-going challenges and a future vision for designing and supporting ocean observational networks. *Frontiers in Marine Science*, *6–2019*, 417. https://doi.org/10.3389/fmars.2019.00417

Gahtan, J., Knapp, K. R., Schreck, C. J. I., Diamond, H. J., Kossin, J. P., & Kruk, M. C. (2024). International best track archive for climate stewardship (IBTrACS) project, version 4.01 [Dataset]. *NOAA National Centers for Environmental Information*. https://doi.org/10.25921/82ty-9e16

Gaspar, P., Gregoris, Y., & Lefevre, J. (1990). A simple eddy kinetic-energy model for simulations of the oceanic vertical mixing—Tests at station Papa and long-term upper ocean study site. *Journal of Geophysical Research*, *95*(C9), 16179–16193. https://doi.org/10.1029/jc095ic09p16179

Geer, A. J. (2021). Learning Earth system models from observations: Machine learning or data assimilation? *Philosophical Transactions of the Royal Society A: Mathematical, Physical and Engineering Sciences*, *379*(2194), 20200089. https://doi.org/10.1098/rsta.2020.0089

Gelaro, R., & Zhu, Y. (2009). Examination of observation impacts derived from observing system experiments (OSEs) and adjoint models. *Tellus A: Dynamic Meteorology and Oceanography*, *61*(2), 179–193. https://doi.org/10.1111/j.1600-0870.2008.00388.x

Gent, P., & McWilliams, J. (1990). Isopycnal mixing in ocean circulation models. *Journal of Physical Oceanography*, *20*(1), 150–155. https://doi.org/10.1175/1520-0485(1990)020<0150:imiocm>2.0.co;2

Gent, P., Willebrand, J., McDougall, T., & McWilliams, J. (1995). Parameterizing eddy-induced tracer transports in ocean circulation models. *Journal of Physical Oceanography*, *25*(4), 463–474. https://doi.org/10.1175/1520-0485(1995)025<0463:peitti>2.0.co;2

Giorgi, F., & Gao, X.-J. (2018). Regional Earth system modeling: Review and future directions. *Atmospheric and Oceanic Science Letters*, *11*(2), 189–197. https://doi.org/10.1080/16742834.2018.1452520

Good, S. A., Martin, M. J., & Rayner, N. A. (2013). EN4: Quality controlled ocean temperature and salinity profiles and monthly objective analyses with uncertainty estimates. *Journal of Geophysical Research: Oceans*, *118*(12), 6704–6716. https://doi.org/10.1002/2013jc009067

Gopalakrishnan, G., Cornuelle, B. D., Hoteit, I., Rudnick, D. L., & Owens, W. B. (2013). State estimates and forecasts of the loop current in the Gulf of Mexico using the MITgcm and its adjoint. *Journal of Geophysical Research: Oceans*, *118*(7), 3292–3314. https://doi.org/10.1002/jgrc.20239

Gopalakrishnan, G., Hoteit, I., Cornuelle, B. D., & Rudnick, D. L. (2019). Comparison of 4DVAR and EnKF state estimates and forecasts in the Gulf of Mexico. *Quarterly Journal of the Royal Meteorological Society*, *145*(721), 1354–1376. https://doi.org/10.1002/qj.3493

Griffies, S., & Hallberg, R. (2000). Biharmonic friction with a smagorinsky-like viscosity for use in large-scale eddy-permitting ocean models. *Monthly Weather Review*, *128*(8), 2935–2946. https://doi.org/10.1175/1520-0493(2000)128<2935:bfwasl>2.0.co;2

Harrop, C., Samtrahan, Christinaholt, & Brown, T. (2017). christopherwharrop/rocoto: Rocoto 1.2.4. https://doi.org/10.5281/zenodo.890939

Heng, B. P., Tubbs, R., Huang, X.-Y., Macpherson, B., Barker, D. M., Boyd, D. F., et al. (2020). SINGV-DA: A data assimilation system for convective-scale numerical weather prediction over Singapore. *Quarterly Journal of the Royal Meteorological Society*, *146*(729), 1923–1938. https://doi.org/10.1002/qj.3774

Hersbach, H., Bell, B., Berrisford, P., Biavati, G., Horanyi, A., Munoz Sabater, J., et al. (2023a). ERA5 hourly data on pressure levels from 1940 to present [Dataset]. *Copernicus Climate Change Service (C3S) Climate Data Store (CDS)*. https://doi.org/10.24381/cds.bd0915c6

Hersbach, H., Bell, B., Berrisford, P., Biavati, G., Horanyi, A., Munoz Sabater, J., et al. (2023b). ERA5 hourly data on single levels from 1940 to present [Dataset]. *Copernicus Climate Change Service (C3S) Climate Data Store (CDS)*. https://doi.org/10.24381/cds.adbb2d47

Hersbach, H., Bell, B., Berrisford, P., Hirahara, S., Horányi, A., Muñoz-Sabater, J., et al. (2020). The ERA5 global reanalysis. *Quarterly Journal of the Royal Meteorological Society*, *146*(730), 1999–2049. https://doi.org/10.1002/qj.3803

Hill, C., DeLuca, C., Balaji, V., Suarez, M., & Silva, A. (2004). The architecture of the Earth system modeling framework. *Computing in Science & Engineering*, *6*(1), 18–28. https://doi.org/10.1109/mcise.2004.1255817

Holland, W. (1978). Role of mesoscale eddies in general circulation of ocean—Numerical experiments using a wind-driven quasi-geostrophic model. *Journal of Physical Oceanography*, *8*(3), 363–392. https://doi.org/10.1175/1520-0485(1978)008<0363:tromei>2.0.co;2

Hoteit, I., Hoar, T., Gopalakrishnan, G., Collins, N., Anderson, J., Cornuelle, B., et al. (2013). A MITgcm/DART ensemble analysis and prediction system with application to the Gulf of Mexico. *Dynamics of Atmospheres and Oceans*, *63*, 1–23. https://doi.org/10.1016/j.dynatmoce.2013.03.002

Hoteit, I., Luo, X., Bocquet, M., Kohl, A., & Ait-El-Fquih, B. (2018). Data assimilation in oceanography: Current status and new directions. In *New frontiers in operational oceanography* (pp. 465–512).

Hoteit, I., Pham, D.-T., Gharamti, M., & Luo, X. (2015). Mitigating observation perturbation sampling errors in the stochastic EnKF. *Monthly Weather Review*, *143*(7), 2918–2936. https://doi.org/10.1175/mwr-d-14-00088.1

Iacono, M. J., Delamere, J. S., Mlawer, E. J., Shephard, M. W., Clough, S. A., & Collins, W. D. (2008). Radiative forcing by long-lived greenhouse gases: Calculations with the AER radiative transfer models. *Journal of Geophysical Research*, *113*(D13). https://doi.org/10.1029/2008jd009944

Ingleby, B., & Huddleston, M. (2007). Quality control of ocean temperature and salinity profiles—Historical and real-time data. *Journal of Marine Systems*, *65*(1–4), 158–175. https://doi.org/10.1016/j.jmarsys.2005.11.019

Kain, J. S. (2004). The Kain–Fritsch convective parameterization: An update. *Journal of Applied Meteorology*, *43*(1), 170–181. https://doi.org/10.1175/1520-0450(2004)043<0170:tkcpau>2.0.co;2

Karspeck, A. R., Danabasoglu, G., Anderson, J., Karol, S., Collins, N., Vertenstein, M., et al. (2018). A global coupled ensemble data assimilation system using the community Earth system model and the data assimilation research testbed. *Quarterly Journal of the Royal Meteorological Society*, *144*(717), 2404–2430. https://doi.org/10.1002/qj.3308

Knapp, K. R., Kruk, M. C., Levinson, D. H., Diamond, H. J., & Neumann, C. J. (2010). The international best track archive for climate stewardship (IBTrACS) unifying tropical cyclone data. *Bulletin of the American Meteorological Society*, *91*(3), 363–376. https://doi.org/10.1175/2009bams2755.1

Knudsen, P., Andersen, O., & Maximenko, N. (2021). A new ocean mean dynamic topography model, derived from a combination of gravity, altimetry and drifter velocity data. *Advances in Space Research*, *68*(2), 1090–1102. https://doi.org/10.1016/j.asr.2019.12.001

Laloyaux, P., Balmaseda, M., Dee, D., Mogensen, K., & Janssen, P. (2016). A coupled data assimilation system for climate reanalysis. *Quarterly Journal of the Royal Meteorological Society*, *142*(694), 65–78. https://doi.org/10.1002/qj.2629

Large, W., Danabasoglu, G., Doney, S., & McWilliams, J. (1997). Sensitivity to surface forcing and boundary layer mixing in a global ocean model: Annual-mean climatology. *Journal of Physical Oceanography*, *27*(11), 2418–2447. https://doi.org/10.1175/1520-0485(1997)027<2418:stsfab>2.0.co;2

Large, W. G., McWilliams, J. C., & Doney, S. C. (1994). Oceanic vertical mixing: A review and a model with a nonlocal boundary layer parameterization. *Reviews of Geophysics*, *32*(4), 363–403. https://doi.org/10.1029/94rg01872

Lea, D., Mirouze, I., Martin, M., King, R., Hines, A., Walters, D., & Thurlow, M. (2015). Assessing a new coupled data assimilation system based on the met office coupled atmosphere–land–ocean–sea ice model. *Monthly Weather Review*, *143*(11), 4678–4694. https://doi.org/10.1175/mwr-d-15-0174.1

Leith, C. (1996). Stochastic models of chaotic systems. *Physica D*, *98*(2–4), 481–491. (15th Annual International Conference of the Center-for-Nonlinear-Studies on Nonlinear Phenomena in Ocean Dynamics, Los Alamos, NM, MAY 15-19, 1995). https://doi.org/10.1016/0167-2789(96)00107-8

Marshall, J., Adcroft, A., Hill, C., Perelman, L., & Heisey, C. (1997). A finite-volume, incompressible Navier Stokes model for studies of the ocean on parallel computers. *Journal of Geophysical Research*, *102*(C3), 5753–5766. https://doi.org/10.1029/96jc02775

Mellor, G., & Yamada, T. (1982). Development of a turbulence closure-model for geophysical fluid problems. *Reviews of Geophysics*, *20*(4), 851–875. https://doi.org/10.1029/rg020i004p00851

Moore, A. M., Martin, M. J., Akella, S., Arango, H. G., Balmaseda, M., Bertino, L., et al. (2019). Synthesis of ocean observations using data assimilation for operational, real-time and reanalysis systems: A more complete picture of the state of the ocean. *Frontiers in Marine Science*, *6*, 90. https://doi.org/10.3389/fmars.2019.00090

Morrison, H., Thompson, G., & Tatarskii, V. (2009). Impact of cloud microphysics on the development of trailing stratiform precipitation in a simulated squall line: Comparison of one-and two-moment schemes. *Monthly Weather Review*, *137*(3), 991–1007. https://doi.org/10.1175/2008mwr2556.1

Naeije, M., Schrama, E., & Scharroo, R. (2000). The radar altimeter database system project RADS. In *IGARSS 2000. IEEE 2000 International Geoscience and Remote Sensing Symposium. Taking the Pulse of the Planet: The Role of Remote Sensing in Managing the Environment. Proceedings (cat. no. 00ch37120)* (Vol. 2, pp. 487–490).

Nakanishi, M., & Niino, H. (2004). An improved Mellor–Yamada level-3 model with condensation physics: Its design and verification. *Boundary-Layer Meteorology*, *112*(1), 1–31. https://doi.org/10.1023/b:boun.0000020164.04146.98

Nakanishi, M., & Niino, H. (2009). Development of an improved turbulence closure model for the atmospheric boundary layer. *Journal of the Meteorological Society of Japan. Series II*, *87*(5), 895–912. https://doi.org/10.2151/jmsj.87.895

NCEP. (2008). *NCEP ADP global upper air and surface weather observations (PREPBUFR format)*. National Geophysical Data Center, NOAA. https://doi.org/10.5064/Z83F-N512

Noh, Y.-C., Chung, E.-S., Choi, Y., Song, H.-J., Raeder, K., & Kim, J.-H. (2025). Application of the satellite-based spectral relationship to the vertical localization for the microwave humidity sounder in the ensemble Kalman filter. *IEEE Transactions on Geoscience and Remote Sensing*.

Pacanowski, R., & Philander, S. (1981). Parameterization of vertical mixing in numerical models of tropical oceans. *Journal of Physical Oceanography*, *11*(11), 1443–1451. https://doi.org/10.1175/1520-0485(1981)011<1443:povmin>2.0.co;2

Parrish, D. F., & Derber, J. C. (1992). The national meteorological center's spectral statistical-interpolation analysis system. *Monthly Weather Review*, *120*(8), 1747–1763. https://doi.org/10.1175/1520-0493(1992)120<1747:tnmcss>2.0.co;2

Penny, S., Akella, S., Alves, O., Bishop, C., Buehner, M., Chevallier, M., et al. (2017). *Coupled data assimilation for integrated Earth system analysis and prediction: Goals, challenges and recommendations, WWRP 2017-3*. World Meteorological Organization. Retrieved from https://library.wmo.int/idurl/4/57666

Raeder, K., Anderson, J. L., Collins, N., Hoar, T. J., Kay, J. E., Lauritzen, P. H., & Pincus, R. (2012). DART/CAM: An ensemble data assimilation system for CESM atmospheric models. *Journal of Climate*, *25*(18), 6304–6317. https://doi.org/10.1175/jcli-d-11-00395.1

Redi, M. (1982). Oceanic isopycnal mixing by coordinate rotation. *Journal of Physical Oceanography*, *12*(10), 1154–1158. https://doi.org/10.1175/1520-0485(1982)012<1154:oimbcr>2.0.co;2

Samrat, N., Candy, B., Lewis, O., Cotton, J., Smith, F., Halloran, G., et al. (2025). Observation impact evaluation through data denial experiments in the Met Office global numerical weather prediction system. *Quarterly Journal of the Royal Meteorological Society*, *151*(771), e5002. https://doi.org/10.1002/qj.5002

Sanikommu, S., Langodan, S., Dasari, H. P., Zhan, P., Krokos, G., Abualnaja, Y. O., et al. (2023). Making the case for high-resolution regional ocean reanalyses: An example with the Red Sea. *Bulletin of the American Meteorological Society*, *104*(7), E1241–E1264. https://doi.org/10.1175/BAMS-D-21-0287.1

Sanikommu, S., Toye, H., Zhan, P., Langodan, S., Krokos, G., Knio, O., & Hoteit, I. (2020). Impact of atmospheric and model physics perturbations on a high-resolution ensemble data assimilation system of the Red Sea. *Journal of Geophysical Research: Oceans*, *125*(8), e2019JC015611. https://doi.org/10.1029/2019jc015611

Sanikommu, S., Wang, Y., El Gharamti, M., Mazloff, M., Verdy, A., Raboudi, N., et al. (2025). Evaluating a hybrid ensemble data assimilative coupled physical-biogeochemical ecosystem model of the Red Sea. *Journal of Advances in Modeling Earth Systems*, *17*(12), e2025MS005086. https://doi.org/10.1029/2025ms005086

Schepers, D., de Boisséson, E., Eresmaa, R., Lupu, C., & de Rosnay, P. (2018). CERA-SAT: A coupled satellite-era reanalysis. *ECMWF Newsletter*, *155*, 32–37.

Skamarock, W., Klemp, J., Dudhia, J., Gill, D., Liu, Z., Berner, J., et al. (2019). A description of the advanced research WRF model version 4. *National Center for Atmospheric Research*, *145*(145), 550.

Smagorinsky, J., Galperin, B., & Orszag, S. (1993). Large eddy simulation of complex engineering and geophysical flows. *Evolution of Physical Oceanography*, 3–36.

Sun, R., Cobb, A., Villas Bôas, A. B., Langodan, S., Subramanian, A. C., Mazloff, M. R., et al. (2023). Waves in SKRIPS: WAVEWATCH III coupling implementation and a case study of tropical cyclone Mekunu. *Geoscientific Model Development*, *16*(12), 3435–3458. https://doi.org/10.5194/gmd-16-3435-2023

Sun, R., Sanikommu, S., Subramanian, A. C., Mazloff, M. R., Cornuelle, B. D., Gopalakrishnan, G., et al. (2024). Enhanced regional ocean ensemble data assimilation through atmospheric coupling in the SKRIPS model. *Ocean Modelling*, *191*, 102424. https://doi.org/10.1016/j.ocemod.2024.102424

Sun, R., Subramanian, A. C., Miller, A. J., Mazloff, M. R., Hoteit, I., & Cornuelle, B. D. (2019). SKRIPS v1.0: A regional coupled ocean–atmosphere modeling framework (MITgcm–WRF) using ESMF/NUOPC, description and preliminary results for the Red Sea. *Geoscientific Model Development*, *12*(10), 4221–4244. https://doi.org/10.5194/gmd-12-4221-2019

Sun, R., Subramanian, A. C., Wolding, B. O., Hsu, T. Y., Mazloff, M. R., Cornuelle, B. D., et al. (2026). Sensitivity of the 2023 Asian summer monsoon water vapor transport to Arabian Sea surface temperature anomalies. *Journal of Geophysical Research: Atmospheres*, *131*(7), e2025JD044185.

Tewari, M., Chen, F., Wang, W., Dudhia, J., LeMone, M., Mitchell, K., et al. (2004). Implementation and verification of the unified NOAH land surface model in the WRF model. In *20th Conference on Weather Analysis and Forecasting/16th Conference on Numerical Weather Prediction* (Vol. 1115).

Toye, H., Zhan, P., Gopalakrishnan, G., Kartadikaria, A. R., Huang, H., Knio, O., & Hoteit, I. (2017). Ensemble data assimilation in the Red Sea: Sensitivity to ensemble selection and atmospheric forcing. *Ocean Dynamics*, *67*(7), 915–933. https://doi.org/10.1007/s10236-017-1064-1

Von Storch, H., & Zwiers, F. W. (2001). *Statistical analysis in climate research*. Cambridge University Press.

Wang, Z., Zhao, J., Huang, H., & Wang, X. (2022). A review on the application of machine learning methods in tropical cyclone forecasting. *Frontiers in Earth Science*, *10*, 902596. https://doi.org/10.3389/feart.2022.902596

Wilks, D. S. (2011). *Statistical methods in the atmospheric sciences* (Vol. 100). Academic Press.

Winterfeldt, J., Geyer, B., & Weisse, R. (2011). Using QuikSCAT in the added value assessment of dynamically downscaled wind speed. *International Journal of Climatology*, *31*(7), 1028–1039. https://doi.org/10.1002/joc.2105

Yao, F., Hoteit, I., Pratt, L. J., Bower, A. S., Zhai, P., Koehl, A., & Gopalakrishnan, G. (2014). Seasonal overturning circulation in the Red Sea: 1. Model validation and summer circulation. *Journal of Geophysical Research-Oceans*, *119*(4), 2238–2262. https://doi.org/10.1002/2013jc009004

Zhang, S., Liu, Z., Zhang, X., Wu, X., Guijun, H., Zhao, Y., et al. (2020). Coupled data assimilation and parameter estimation in coupled ocean–atmosphere models: A review. *Climate Dynamics*, *54*(11–12), 5127–5144. https://doi.org/10.1007/s00382-020-05275-6